Author(s): Hellén, E. K. O. & Alava, Mikko J. & Niskanen, K. J.

Title: Porous structure of thick fiber webs

Year: 1997

Version: Final published version

Please cite the original version:

Hellén, E. K. O. & Alava, Mikko J. & Niskanen, K. J. 1997. Porous structure of thick fiber webs. Journal of Applied Physics. Volume 81, Issue 9. 6425-6431. ISSN 0021-8979 (printed). DOI: 10.1063/1.364423.

AIP | Journal of Applied Physics

Porous structure of thick fiber webs

E. K. O. Hellén, M. J. Alava, and K. J. Niskanen

Citation: Journal of Applied Physics **81**, 6425 (1997); doi: 10.1063/1.364423
View online: http://dx.doi.org/10.1063/1.364423
View Table of Contents: http://scitation.aip.org/content/aip/journal/jap/81/9?ver=pdfcov
Published by the AIP Publishing

Porous structure of thick fiber webs

E. K. O. Hellén and M. J. Alava[a)]
Laboratory of Physics, Helsinki University of Technology, P.O. Box 1100, FIN-02015, HUT, Finland

K. J. Niskanen
KCL Paper Science Centre, P.O. Box 70, FIN-02151 Espoo, Finland

(Received 22 October 1996; accepted for publication 20 January 1997)

The bulk properties and stochastic pore geometry of finite-thickness fiber webs are studied using a realistic model for the sedimentation of flexible fibers [K. J. Niskanen and M. J. Alava, Phys. Rev. Lett. **73**, 3475 (1994)]. The resulting web structure is controlled by a dimensionless number $F=T_f w_f/t_f$, where T_f is fiber flexibility, w_f fiber width, and t_f fiber thickness. The fiber length ($\gg w_f, t_f$) is irrelevant. With increasing coverage $\overline{c}$, a crossover occurs at $\overline{c}=c_0\approx 1+2F$ from a vacancy-controlled two-dimensional (2D) structure to a pore-controlled 3D structure. The 3D structures are isomorphic in that the pore dimensions are exponentially distributed, with the decay rate dependent only on F. © *1997 American Institute of Physics.* [S0021-8979(97)04809-3]

I. INTRODUCTION

The mechanical and transport properties of disordered materials depend on their geometry. The simplest systems are two-phase materials, e.g. porous metals and particle aggregates that consist of a solid phase and a *pore* phase. Such structures are dual in that properties such as conductivity and elastic modulus depend on the solid phase[1–4] while others such as permeability depend on the pore phase. Linear behavior with the pore volume fraction is expected in, e.g., resistivity at low porosity and in permeability at high porosity. Nonlinear phenomena should take place close to the percolation threshold of the governing phase-pores in fluid flow and solid phase in transport problems.

The connection between the dynamical properties and the structure is difficult to establish because higher-order statistics of the medium geometry are needed.[5] In analytical calculations one has to resort to approximations such as variational bounds using second and third order correlation functions,[6] effective medium techniques applied at the ''best length scale''[7–10] and percolation-type ideas.[11,12] As an example, consider permeability. If the pore system is well-connected then the capillary approximation should hold. Thus the permeability depends only on the effective hydraulic radius of a typical pore and the contact angle of the fluid phase.[13,14] However, the capillary approximation is not useful if the pore system consists of large cavities that are connected through narrow pore throats. It may then be useful to relate the distribution of the throats to the percolation threshold in connectivity.[11,12,15]

Analytical calculations for dynamic properties can be tested using numerically simulated model structures. In real world disordered solids can be formed through deposition or sedimentation of solid particles from a suspension but little is known about the structure of such systems[16] since it depends on particle interactions in the suspension and during the settling process.[17] We have recently introduced a computationally effective model for the geometry of sedimented random fiber networks.[18] In the model suspension flow and particle interactions are ignored. The fibers settle down one by one and do not deform the already formed underlying structure. The three-dimensional geometry is governed by the flexibility and dimensions of the fibers.

The simulation model produces realistic porous structures that closely resemble manmade fibrous webs such as paper and nonwovens. Indeed, paper has been used as a model random material in imbibition experiments in the statistical physics communitity to study invasion percolation and kinetic roughening.[19] The model can also be extended to other sedimentation processes with different particle shapes. All structures formed through sedimentation from a dilute suspension of non-interacting particles are governed by Poisson statistics. Our model captures their essential features.

In this article, we have applied the model to the geometrical properties of ''thick'' planar random fiber webs. In addition to macroscopic quantities such as the average porosity and coordination number, we characterize the pore population in the vertical and planar directions of the web. The results are summarized with empirical formulas and compared with the Poissonian statistics. The rest of this paper is organized as follows. The simulation model is introduced in Sec. II. Bulk properties are discussed in Sec. III and pore statistics in Sec. IV. Permeability of the web is briefly discussed in Sec. V and conclusions are presented in Sec. VI.

II. THE DEPOSITION MODEL

We start with a two-dimensional square lattice substrate, of dimension $L=10...1000$. L is important only for nontrivial scaling quantities as the surface roughness and percolation threshold, which involve correlations parallel to the substrate. Such properties are not considered here. We concentrate on long ($l_f \gg 1$) straight fibers of width $w_f=1$ equal to the lattice constant. Fiber thickness t_f is arbitrary in our study.[20] Fibers are positioned at random in the two lattice directions so that local coverage c (number of fibers covering any cell) is an integer. Periodic boundary conditions are applied to fibers that cross the boundaries.[18]

[a)]Also at: Department of Physics and Astronomy, Michigan State University, East Lansing, MI 48824-1116; Electronic mail: mja@fyslab.hut.fi

Porous structures arise when the fibers have a nonzero stiffness. A bending flexibility T_f of the fibers is defined through a constraint on the height of ''steps'' that the fibers can form:

$$|z_i - z_j| \leqslant T_f, \tag{1}$$

where z_i and z_j are the elevations of the top surface of the fiber above any two nearest neighbor cells i and j covered by the fiber. Every new fiber is pressed down as low as possible without deforming the underlying web and while still obeying Eq. (1).

The spatial discretization should have no effect on the web properties except when T_f is an integer multiple of fiber thickness. The resulting irregularities will be pointed out below. They could be avoided by assigning a range of incommensurate values to, e.g., fiber flexibility. One can demonstrate that at fiber lengths $l_f \gg w_f$ the structure becomes independent of l_f. It is then easy to accept that the web structure should depend only on a dimensionless flexibility number[18]

$$F = T_f w_f / t_f. \tag{2}$$

We have checked through simulations that this is the case.[21] Our data indicates that $l_f/w_f > 20$ is sufficient to reach the F-controlled regime. Of course, the thickness and pore heights of the web are proportional to t_f.

Given that only F matters, all the simulations reported below have been made with $w_f = t_f = 1$. A high F leads to a dense web and a low F to a porous one. To connect with the real world the so-called wet fiber flexibility[22] (WFF) of paper-making fibers can be related to T_f through $T_f = [C \times w_f \times WFF]^{1/4}$, where C depends on the pressure and other experimental details. Measured values of WFF[23] and known dimensions of paper-making fibers yield $F = 0.5 \ldots 3$.

Our model is similar to many growth models and particularly to the Vold model.[24,25] At the same time it ignores many real sedimentation phenomena such as clustering or flocculation of the fibers and reordering along the surface because of hydrodynamic or gravitational forces.[17] The local interactions are replaced by an average force accounted for by F. The simple bending rule, Eq. (1), does not even describe accurately hydrostatic compression.[26] Despite all these simplifications the model seems powerful in producing realistic structures.

III. BULK PROPERTIES: DENSITY AND CONNECTIVITY

The bulk properties of fiber webs can be characterized by four numbers, coverage $\overline{c}$, density ρ, coordination number $\overline{n}$ and pore number $\overline{p}$. Coverage $\overline{c}$ is the average number of fibers at any point. In most of our simulations $\overline{c} = 50 - 100$. Density $\rho \leqslant 1$ is the volume fraction occupied by the fibers; hence ρ is equivalent to solid fraction ϕ in porosity language. The volume of the web is bounded by the rough surfaces. The web thickness is the average of local thicknesses. Apparent thicknesses that one would measure in practice give a lower bound for ρ. Coordination number $\overline{n}$ specifies the connectivity of the web. We define $\overline{n} \leqslant 1$ as the average contact area, divided by the total area, $2 l_f w_f$, of a fiber.[27] Pore number $\overline{p}$ is the average number of pores per cell area.

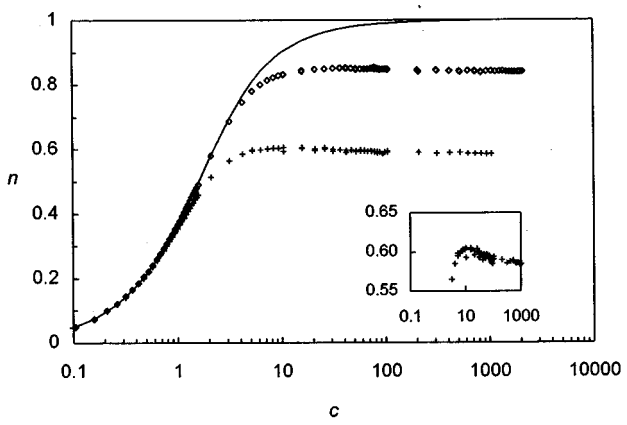

FIG. 1. Coordination number $\overline{n}$ against coverage $\overline{c}$; the solid line gives Eq. (4). $F = 1$ (+) and 2 ($\diamond$), fiber length $l_f = 21$. The inset shows an enlargement of the $F = 1$ case. Two system sizes, $L = 1000$ and 100 (the latter at high coverages), give slightly different results around $\overline{c} = 10$.

Consider first the special case $F = \infty$ when the fibers have infinite flexibility or zero thickness. The web is then two-dimensional. The only ''pores'' are vacancies, cells covered with no fibers. Poisson statistics implies that their number is $\overline{v} = \exp(-\overline{c})$ and the coordination number is given by[28]

$$\overline{n} = 1 - [1 - \exp(-\overline{c})]/\overline{c}. \tag{3}$$

Hence $\overline{n}$ increases with coverage.

With finite flexibility and nonzero thickness, pores develop when coverage increases. It is easy to see that

$$\overline{n} = 1 - \frac{\overline{p} + 1}{\overline{c}} [1 - \exp(-\overline{c})] \tag{4}$$

follows as a generalization of Eq. (3). The coordination number $\overline{n}$ still increases with $\overline{c}$, but only at low $\overline{c}$ (cf. Fig. 1). At higher coverages $\overline{n}$ has a weak maximum, and then becomes constant, $\overline{n} \to n_\infty$. In the following we use the subscript ∞ for the asymptotic high coverage region. This happens because the roughness of the top surface increases so that at some point the new fibers are no longer able to conform with the deepest valleys. Thereafter $\overline{p}$ increases and counteracts the decrease in $\overline{v}$.

Whereas $\overline{n}$ has a maximum with increasing coverage, the web density ρ goes down monotonically (Fig. 2). There is no simple relationship between $\overline{n}$ and ρ at fixed F when $\overline{c}$ varies, but $\overline{n}$ and ρ are almost linearly related when F varies at fixed $\overline{c}$.[18]

In the asympotic high-coverage region the flat substrate no longer has any effect on $\overline{n}$, and every new ''layer'' of fibers has the same structure as the preceding one. This is the region of three dimensional bulk structure. Hence the pore number increases linearly with coverage

$$\overline{p} = p'_\infty (\overline{c} - c_0). \tag{5}$$

The coverage c_0 measures the crossover from a two-dimensional system to the growth of a three-dimensional

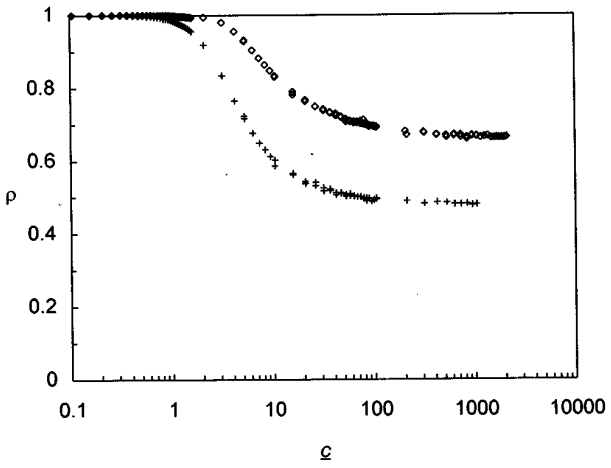

FIG. 2. Density ρ against coverage $\overline{c}$. $F=1$ (+) and 2 ($\diamond$), fiber length $l_f=21$. Two system sizes, $L=1000$ and 100 (the latter at high coverages).

bulk phase. The discrete model geometry causes oscillations in c_0 against F (Fig. 3). If they are smeared out, c_0 is roughly given by

$$c_0 \approx 1+2F. \tag{6}$$

On the average no pores exist at $\overline{c}<1$, thus $c_0 \geqslant 1$. The simulation data for $p'_\infty = 1-n_\infty$, the slope of $\overline{p}$ relative to coverage, is well represented by an *ad hoc* expression

$$p'_\infty = 1-n_\infty \simeq \frac{1-\exp(-2F)}{2F}, \tag{7}$$

similar to Eq. (3) at the 2D limit [Fig. 4(a)]. Figure 4(b) compares the asymptotic density ρ_∞: it is slightly smaller than the coordination number, $n_\infty \approx 1.2\rho_\infty$.

IV. PORE STATISTICS

We show next how the pore system of our model changes when fiber flexibility is changed. Pores are defined as vertical openings between fibers. Cavities, i.e., cells of zero local coverage are extremely rare at the high coverages considered and are excluded from the following analysis

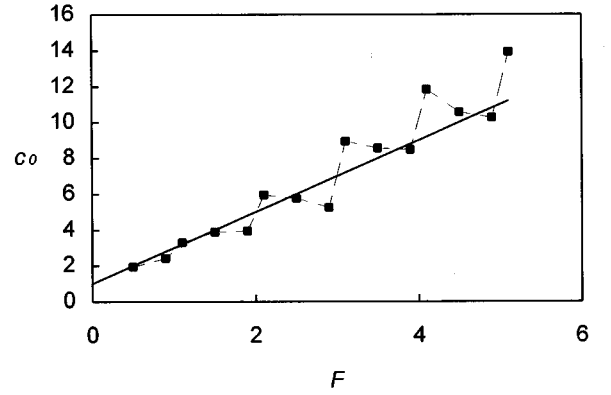

FIG. 3. The 2D-to-3D crossover coverage c_0 against fiber flexibility F. The solid line is $c_0=1+2F$.

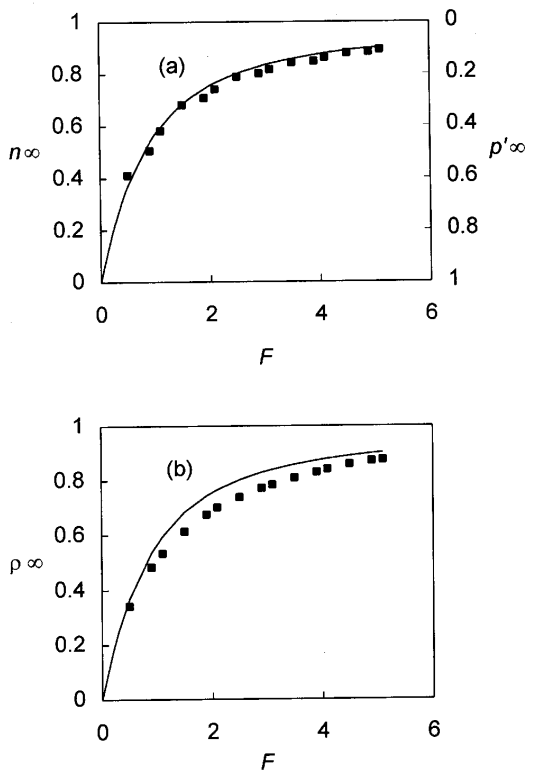

FIG. 4. The asymptotic coordination number, n_∞ [(a), l.h.s.], the coverage gradient of the pore number, p'_∞ [(a), r.h.s.], and the asymptotic density ρ_∞ (b) against fiber flexibility F. The solid lines give the expression $(1-e^{-2F})/2F$.

even if they occurred. Nor is the open space between the web and the substrate considered. The pore network is different in the thickness (or z direction) and xy plane since fibers are long compared to web thickness. The two directions are therefore treated separately.

A. Pore "heights"

Figure 5 illustrates the porous model geometry in the thickness direction. The distribution of pore heights is determined by counting the height of all vertical openings above every cell. This definition, instead of an average height of a pore, avoids all ambiquities regarding what a single pore is.

Figure 6(a) shows two examples of the pore height distribution $G(h)$ at $\overline{c}=83 \gg c_0$. Possible pore height values are determined by F; the values used here, $F=0.2$ and 1.2, mean that all pore heights must be multiples of $0.2t_f$. At that

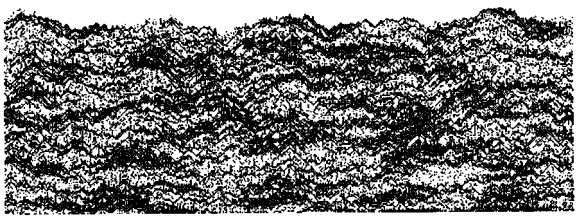

FIG. 5. An example of the cross-section of the fiber web at $\overline{c}=83$. The section is 500 cells wide. Fibers are black and pores white.

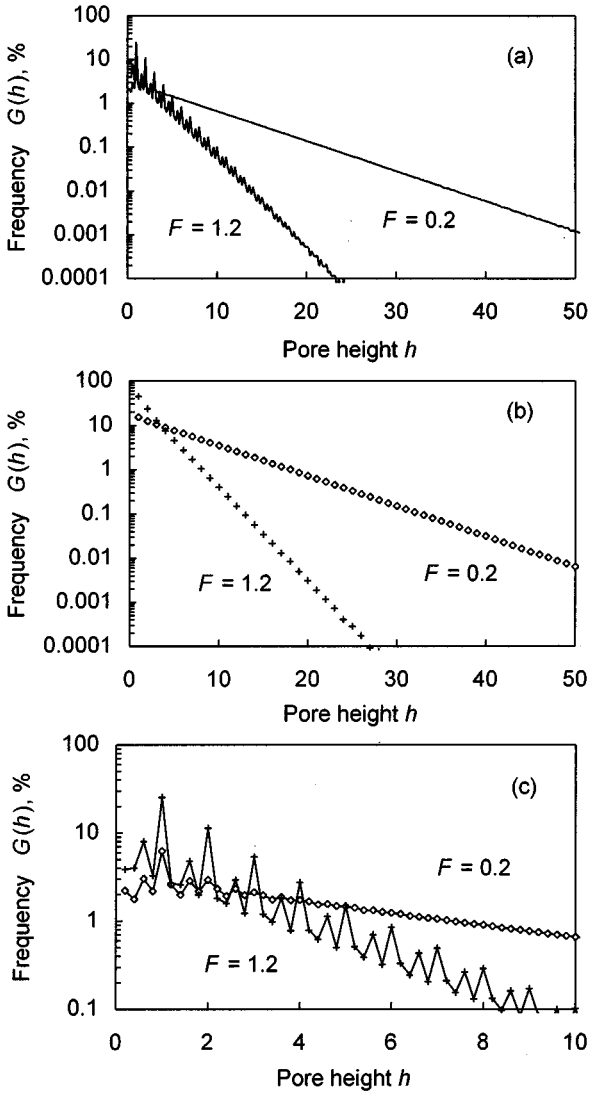

FIG. 6. The distribution of pore heights $G(h)$ for $F=0.2$ (+) and 1.2 ($\diamond$). Pore height h is given in the units of t_f. In (a) all the possible values of h, that is multiples of $0.2t_f$, are included while in (b) $\Sigma_{k=-4}^{0} G(h + 0.2kt_f)$ is plotted for integer h. Coverage $\overline{c} = 83$. (c) shows (a) in more detail.

resolution $G(h)$ oscillates slightly with a cycle of t_f. The oscillations are artefacts of the discrete model. The exponential nature of the distribution function becomes more evident when pore heights are rounded to integer values of t_f, $G \rightarrow \Sigma_{k=-4}^{0} G(h + 0.2kt_f)$, with integer h/t_f [Fig. 6(b)]. The exponential approximation underestimates somewhat the frequency of flat pores [Fig. 6(c)]. If the distribution were precisely exponential,

$$G(h) = h_0^{-1} \exp(-h/h_0), \tag{8}$$

then the average pore height $\overline{h}$ should be equal to h_0. The actual values of $\overline{h}$ are systematically larger than h_0 (Fig. 7). In the limit $\overline{c} \rightarrow \infty$ we expect that $\overline{h} \approx t_f/\rho_\infty$ as the web density ρ_∞ is related to $\overline{h}$ through $\rho_\infty^{-1} = (\overline{c} + \overline{ph})/\overline{c} \approx \overline{h}(1-\rho_\infty) + 1$. However, the simulation results (at $\overline{c} = 83$) do not agree with this. Instead a good

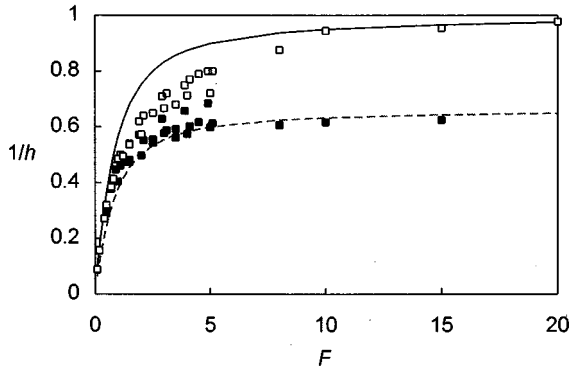

FIG. 7. The inverse values of the average pore height, $1/\overline{h}$ (■), and the decay constant, $1/h_0$ [□, see Eq. (8)], against fiber flexibility F. Pore heights are in the units of t_f. The solid line is equal to n_∞ and the dashed line to $2n_\infty/3$.

approximation is $\overline{h} \approx 1.5t_f/n_\infty$. The discrepancy is caused by the fact that $n_\infty \geqslant \rho_\infty$ (cf. Fig. 4). A similar but not quite as good an approximation applies to h_0: $h_0 \approx t_f/n_\infty$ (Fig. 7).

B. Pore "areas"

Pore areas are determined from xy cross sections within the web (see Fig. 8) for illustration. The pores form a complicated inter-connected system where pores cannot be uniquely defined.

We have considered,[29] three different methods to determine the pore area distribution $P(A)$. In the first one we calculate the fractional area of narrow throats, or constrictions. The throats are those parts of the pore system through which squares of a given size cannot pass along the xy plane. Starting from a single cell we use larger and larger test squares. At each square size we remove the corresponding throats and evaluate the remaining pore area. In the end we have the distribution of total pore area that is xy permeable to squares of a given size. This method gives an upper bound for $P(A)$.

In the second penetration method we determine the largest test square that can go through the xy cross section as well as the total area where this happens. This area is then blocked and the next, smaller test square is used to determine how much of the remaining area that is permeable to them. The method resembles experiments where increasing pressure is used to force a test fluid into ever smaller pores.

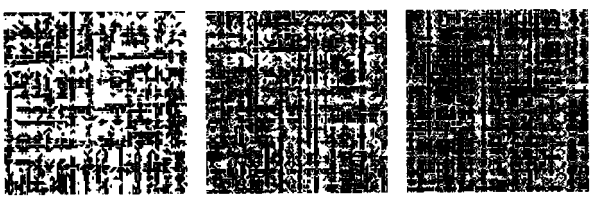

FIG. 8. xy cross sections of 100×100 cells in the middle of a web with $\overline{c}=83$ for fiber flexibility $F=0.2$, 0.3 and 0.6 (from left to right, respectively). Fibers are black and pores white. Fiber width $w_f=3.5$ cells.

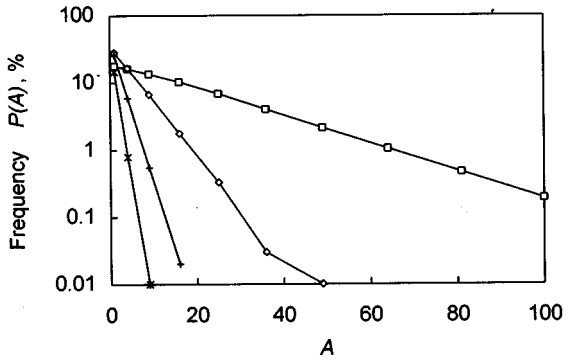

FIG. 9. The distribution of pore areas $P(A)$ for $F=0.4$ (□), 0.9 (◇), 2.1 (+), and 5.1 (★). Pore areas are of the form n^2. Coverage $\bar{c}=83$.

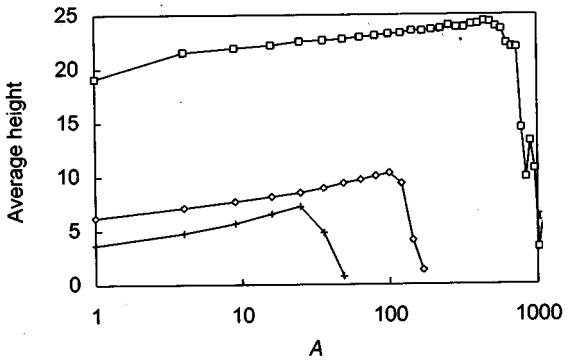

FIG. 11. Characteristic average pore height $\tilde{h}$ against pore area A for $F=0.1$ (□), 0.4 (◇), and 1 (+) as given by the penetration algorithm. Coverage $\bar{c}=83$.

However, the correspondence is not precise as measurements always probe the three dimensions simultaneously.

The third method is equivalent to the second one except that we start with one cell as the test square and proceed to larger squares. At each step we move the test square row by row through all the cells. Every time the test square fits into a pore the corresponding cells are blocked. The test cell is then moved forward until it meets the next large enough opening. In this way all pores are covered by at most one test square. The method gives a lower bound for $P(A)$.

Even though the three methods differ in principle, they all give quite similar results. Figure 9 shows the distribution of pore areas $P(A)$, as given by the minimum cross section method (the third method above). The distribution is again close to exponential, $P(A)\sim\exp(-A/A_0)$, with $A_0\sim 1/F$. The average pore area A is somewhat different and given by $\bar{A}\approx 1/n_\infty$ for $w_f=1$ (Fig. 10). The distribution function $P(A)$ has only a few values because A is of the form n^2.

One might expect that pores with a large area A would also be high, but in fact the correlation between pore areas and heights is weak. In Fig. 11 the characteristic height $\tilde{h}(A)$ is the average height of pores that are permeable (in the z-direction) to test squares of area A (the second method above). The fiber flexibility F has no qualitative effect on $\tilde{h}(A)$. At large A there is a sharp cut-off above which $\tilde{h}$ drops to zero; this may be caused by the use of squares as probes. The cut-off area and height are related through $h_{\rm cut}\sim A_{\rm cut}^{1/3}$ when F is varied.

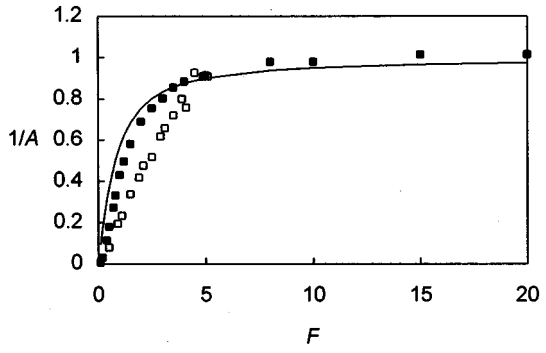

FIG. 10. The inverse values of the average pore area, $1/\bar{A}\bar{h}$ (■), and the decay constant, $1/A_0$ (□), against fiber flexibility F. The solid line is equal to $1/n_\infty$. Pore areas are of the form n^2. Coverage $\bar{c}=83$.

The above observations together with the exponential distributions of pore heights and areas show that the 3D structures are isomorphic. Since the pore height and cross-sectional area are only weakly correlated, the average pore volume $\bar{V}$ can be estimated as $\bar{V}\approx\bar{h}\bar{A}\approx 1.5/n_\infty^2$ since from above $\bar{A}\approx 1/n_\infty$ and $\bar{h}\approx 1.5/n_\infty$. Likewise the average surface area $\bar{S}$ is given by $\bar{S}\approx 2\bar{A}+4\bar{h}\sqrt{\bar{A}}$ assuming the pores are ''ellipsoidal.'' The number of pores per unit volume is $(2/3)n_\infty^2(1-n_\infty)$. Hence the surface area of pores per unit volume of web, or specific surface area, is given by $\bar{s}\approx(4\sqrt{n_\infty}+4n_\infty/3)(1-n_\infty)$ for $\bar{c}\gg 1$. It has a maximum as a function of F [Fig.12(a)].

V. WEB PERMEABILITY

Our model is truly three-dimensional in the following sense. The pores percolate in a 2D-cut parallel to the xy-plane only for $F\ll 1$.[30] In cuts parallel to the xz- or yz-plane pores never percolate but the permeability of the 3D web can still be nonzero. A thorough analysis of the permeability is beyond the scope of this article, but a variational bound in the z-direction can be calculated.

The hydraulic conductance g_h of an individual pore is given by[11,12]

$$g_h(A,h)=\frac{A^2}{8\pi h\eta}, \tag{9}$$

where A is the pore area, h the pore height, and η the fluid viscosity. This expression is used in a variational trial solution

$$g_{\rm var}=g(A,h)(1-\rho)[f(A,h)-f_c]^t, \tag{10}$$

where $f(A,h)=G(h)P(A)$ is the combined pore size distribution (assuming A and h independent) and $f=f_c$ is the percolation boundary in the A,h phase space. The percolation exponent t may differ from the value $t=1.9$ of 3D isotropic systems[11,31] since the pore structure is anisotropic.

The trial solution is minimized with respect to both h and A. The minimum with respect to h is given by

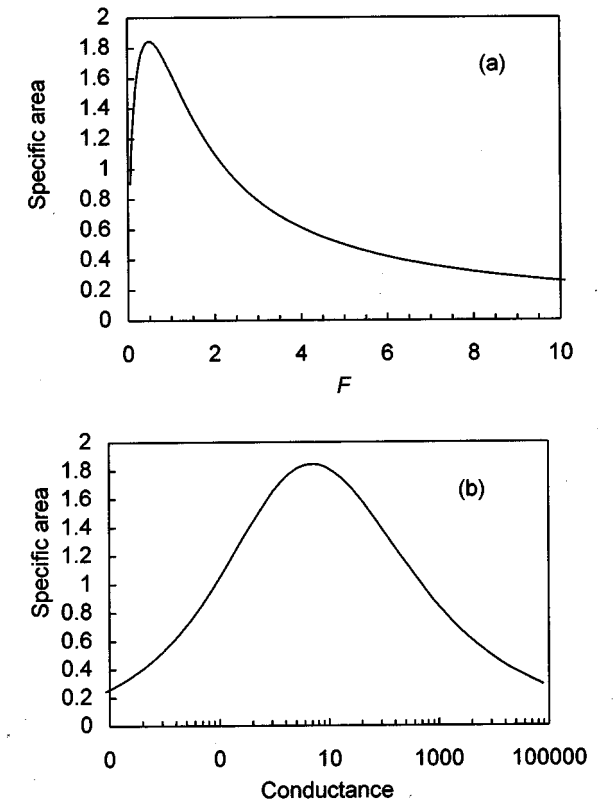

FIG. 12. Specific pore area (i.e., average pore area per unit volume) $\overline{s}$ against fiber flexibility F (a) and hydraulic conductance g (b).

$G(h)P(A)=f_c-th/h_0$ and therefore it is sensitive to the values of f_c and t. However, we can proceed by looking at how the hydraulic conductivity scales with the cross-sectional distribution. We can then assume f_c to be very small—as is appropriate in many continuum problems. The trial solution is minimized at $A=2A_0/t \approx A_0$ if $t=1.9$. Thus the hydraulic conductivity should be proportional to $g\sim A_0^2(1-\rho) \sim (1-\rho)/F^2$. In the asymptotic high coverage region this reduces to [cf. Eq. (7)]

$$g\sim[1-\exp(-2F)]/F^3, \tag{11}$$

illustrated in Fig. 12(b). The plot, particularly the maximum, is interesting since g and $\overline{s}$ can both be measured experimentally.

VI. CONCLUSIONS

We have employed a simple numerical algorithm to study the structure of sedimented fiber webs when coverage and fiber flexibility vary. The effects of fiber flexibility are described by the dimensionless parameter F. At low coverages the system is effectively two-dimensional and its statistical geometry is well understood.[28] With increasing coverage, a three-dimensional bulk phase starts to grow above a critical coverage $c_0=1+2F$. The 3D bulk phase in the asymptotic high coverage region is isomorphic in structure, qualitatively independent of the fiber properties. The distributions characterizing pore sizes are roughly exponential with the decay rate inversely proportional to the asymptotic coordination number n_∞. The coordination number $\overline{n}$ is in turn a monotonically increasing function of F. The frequency and size of pores decrease when F increases.

The square lattice geometry should suffice to describe, e.g., mechanical properties and conductivity of fiber webs that are related to the average coordination number. However, the pore size distributions considered above are limited to length scales close to fiber width and thickness. In real systems, such as paper, much smaller lengths are often relevant. Small pores are controlled by fiber shape and internal pores and perhaps by local surface tension and other forces acting on and between the fibers. Such effects are not included in our model. Thus the model would probably fail to represent correctly the permeability of continuous systems.

Our model can be applied to study multicomponent systems. Technologically interesting are, e.g., grainlike objects dispersed in a fiber web and (perhaps correlated) distributions of fiber length and flexibility.

ACKNOWLEDGMENTS

This study was supported by the Technology Development Centre of Finland and the Academy of Finland. We are grateful to Niko Nilsen and Lauri Salminen for assistance.

[1] *Statistical Models for the Fracture of Disordered Media*, edited by H. J. Herrmann and S. Roux (North-Holland, Amsterdam, 1990).
[2] M. Sahimi, Physica A **186**, 160 (1992).
[3] S. Kirkpatrick, Rev. Mod. Phys. **45**, 574 (1973).
[4] L. M. Schwartz, S. Feng, M. F. Thorpe, and P. N. Sen, Phys. Rev. **32**, 4607 (1985).
[5] S. Torquato, Appl. Mech. Rev. **44**, 37 (1991).
[6] D. A. Coker and S. Torquato, J. Appl. Phys. **77**, 6087 (1995).
[7] R. Hilfer, Phys. Rev. B **44**, 60 (1991).
[8] R. Hilfer, Phys. Rev. B **45**, 7115 (1992).
[9] E. Haslund, B. D. Hansen, R. Hilfer, and B. Nost, J. Appl. Phys. **76**, 5473 (1994).
[10] B. Virgin, E. Haslund, and R. Hilfer, preprint cond-mat/9605004.
[11] A. J. Katz and A. H. Thompson, Phys. Rev. B **34**, 8179 (1986).
[12] J. R. Banavar and D. L. Johnson, Phys. Rev. B **35**, 7283 (1987).
[13] A. E. Scheidegger, *The Physics of Flow through Porous Media* (University of Toronto Press, Toronto, 1974).
[14] M. Sahimi, Rev. Mod. Phys. **65**, 1406 (1993).
[15] L. M. Hirsch and A. H. Thompson, Phys. Rev. E **50**, 2069 (1994).
[16] M. L. Kurnaz and J. V. Maher, Phys. Rev. E **53**, 978 (1996).
[17] I. Pagonabarraga and M. Rubi, Phys. Rev. Lett. **73**, 114 (1994).
[18] K. J. Niskanen and M. J. Alava, Phys. Rev. Lett. **73**, 3475 (1994).
[19] A.-L. Barabasi and H. E. Stanley, *Fractal Concepts in Surface Growth* (Cambridge University Press, Cambridge, 1995).
[20] For paper-making fibers $l_f/t_f \geqslant l_f/w_f \simeq 20-100$.
[21] N. V. Nilsen and K. J. Niskanen, internal report of KCL (1995).
[22] R. Steadman and P. Luner, *Papermaking Raw Materials*, edited by V. Punton (Mechanical Engineering Publ. Ltd., London, 1985), pp. 311–338.
[23] L. Paavilainen, Paperi ja Puu **46**, 689 (1993).
[24] M. J. Vold, J. Colloid Interface Sci. **14**, 168 (1959).
[25] J. Krug and H. Spohn, in *Solids far from Equilibrium: Growth, Morphology, Defects*, edited by C. Godréche (Cambridge University Press, Cambridge, 1991), pp. 479–582.
[26] J. D. Sherwood and H. Van Damme, Phys. Rev. E **50**, 3834 (1994).
[27] For paper the quantity corresponding to coordination number is relative

bonded area, RBA. See O. J. Kallmes, H. Corte, and G. Bernier, Tappi J. **46**, 502 (1963).
[28] H. Corte and O. J. Kallmes, Tappi J. **43**, 737 (1960).
[29] These rather *ad hoc* algorithms are also related to the concept of lineal path, see B. Lu and S. Torquato, Phys. Rev. A **45**, 922 (1992).
[30] N. Martys and E. J. Garboczi, Phys. Rev. B **46**, 6080 (1992).
[31] This calculation is a version of the standard AHL argument, V. Ambegaokar, B. I. Halperin, and J. S. Langer, Phys. Rev. B **4**, 2612 (1971).